

## **Target Size Variation in Microdosimetric Distributions and its Impact on the Linear-Quadratic Parameterization of Cell Survival**

Authors: Villegas, Fernanda, Tilly, Nina, and Ahnesjö, Anders

Source: Radiation Research, 190(5) : 504-512

Published By: Radiation Research Society

URL: <https://doi.org/10.1667/RR15089.1>

---

BioOne Complete ([complete.BioOne.org](https://complete.BioOne.org)) is a full-text database of 200 subscribed and open-access titles in the biological, ecological, and environmental sciences published by nonprofit societies, associations, museums, institutions, and presses.

Your use of this PDF, the BioOne Complete website, and all posted and associated content indicates your acceptance of BioOne's Terms of Use, available at [www.bioone.org/terms-of-use](https://www.bioone.org/terms-of-use).

Usage of BioOne Complete content is strictly limited to personal, educational, and non - commercial use. Commercial inquiries or rights and permissions requests should be directed to the individual publisher as copyright holder.

---

BioOne sees sustainable scholarly publishing as an inherently collaborative enterprise connecting authors, nonprofit publishers, academic institutions, research libraries, and research funders in the common goal of maximizing access to critical research.

# Target Size Variation in Microdosimetric Distributions and its Impact on the Linear-Quadratic Parameterization of Cell Survival

Fernanda Villegas,<sup>a,1</sup> Nina Tilly<sup>a,b</sup> and Anders Ahnesjö<sup>a</sup>

<sup>a</sup> Medical Radiation Physics, Department of Immunology, Genetics and Pathology, Uppsala University, Akademiska Sjukhuset, Uppsala SE-75185, Sweden; and <sup>b</sup> Elekta Instrument AB, Stockholm SE-10393, Sweden

Villegas, F., Tilly, N. and Ahnesjö, A. Target Size Variation in Microdosimetric Distributions and its Impact on the Linear-Quadratic Parameterization of Cell Survival. *Radiat. Res.* 190, 504–512 (2018).

The linear-quadratic (LQ) parameterization of survival fraction [SF(*D*)] inherently assumes that all cells in a population receive the same dose (*D*), albeit the distribution of specific energy *z* over the individual cells *f*(*z*,*D*) can be very wide. From these microdosimetric distributions, which are target size dependent, we estimate the size of the cellular sensitive volume by analyzing its influence on the LQ parameterization of cell survival. A Monte Carlo track structure code was used to simulate detailed tracks from a <sup>60</sup>Co source as well as proton and carbon ions of various energies. From these tracks, *f*(*z*,*D*) distributions were calculated for spherical targets with diameters ranging from 10 nm to 12 μm. A cell survival function based on *f*(*z*,*D*) was fitted to experimental LQ α values, revealing an intrinsic limitation that target size imposes on the usage of *f*(*z*,*D*) to describe the linear term of the LQ parameterization. The results indicate that such threshold volume arises naturally from the relationship between the particle's probability of no-hit and the probability of cell survival. Further analysis led to the proposal of a radiobiological property  $\bar{y}_{f,\text{MID}}$ , defined as the mean lineal energy corresponding to the target size that allows equivalence between the mean inactivation dose (MID) and the mean specific energy *z*<sub>1</sub>. The fact that  $\bar{z}_1$  is an increasing continuous function of target size within the range of biological targets of interest in radiobiology, ensures the uniqueness of  $\bar{y}_{f,\text{MID}}$  for any radiation quality, thus, its potential usefulness in modeling. In conclusion, an accurate estimation of such threshold volumes may be useful for improving modeling of cell survival curves. © 2018 by Radiation Research Society

## INTRODUCTION

The clonogenic cell survival assay is a straightforward and inexpensive *in vitro* assay that quantifies the proportion

<sup>1</sup> Address for correspondence: Akademiska Sjukhuset Ing. 82, Avd. Sjukhusfysik, SE-75185, Uppsala, Sweden; email: fernanda.villegas-navarro@igp.uu.se.

of cells that retain reproductive integrity, and thus proliferate to create viable colonies, after irradiation with incremental amounts of dose. The resulting cell survival ratio has been and still is fundamental to the study of biological effects from ionizing radiation. The method most used for describing cell survival data is the so-called linear-quadratic (LQ) parameterization (*I*), where the probability for survival at a dose (*D*) is given by:

$$\text{SF}(D) = e^{-(\alpha D + \beta D^2)} \quad (1)$$

In addition to the trivial Poisson interpretation, that the parameters α and β are proportionality factors for lethal events, a satisfactory bio-mechanistic explanation is still missing. Equation (1) provides a quantification of the integrated response of the cell where many complex intra- and extracellular processes are involved. Indeed, to decouple each process is a colossal task. However, with the advent of particle radiotherapy, there has been a renewed interest in the development of semi-mechanistic mathematical models for prediction of the LQ parameters. Implementation of these models in radiation treatment planning systems would allow optimization of biological effectiveness throughout the treated volume. This is essential, particularly for treatment with heavier ions (e.g., carbon), since the large and rapid change in the relative biological effectiveness (RBE) at the end of the Bragg Peak may pose a serious threat to any healthy tissue located behind (2, 3). In proton therapy, it is common practice to apply a generic constant RBE value of 1.1 (4), however, there are also strong indications of the benefits of implementing variable RBE in clinical planning (5–7).

Micro- and nanodosimetric-based semi-mechanistic models assume the existence of a so-called “sensitive volume,” which is generally conceptualized as the volume within a cell that will most likely induce cell death if affected by the ionizing radiation (8). It is natural to assume that such volume is found within the cell nucleus, as it harbors the DNA molecule, yet there is increasing evidence suggesting induced cell death by compromising other cellular structures (9). The underlying truth is that without knowledge of the subcellular composition of the sensitive volume, it remains unmeasur-

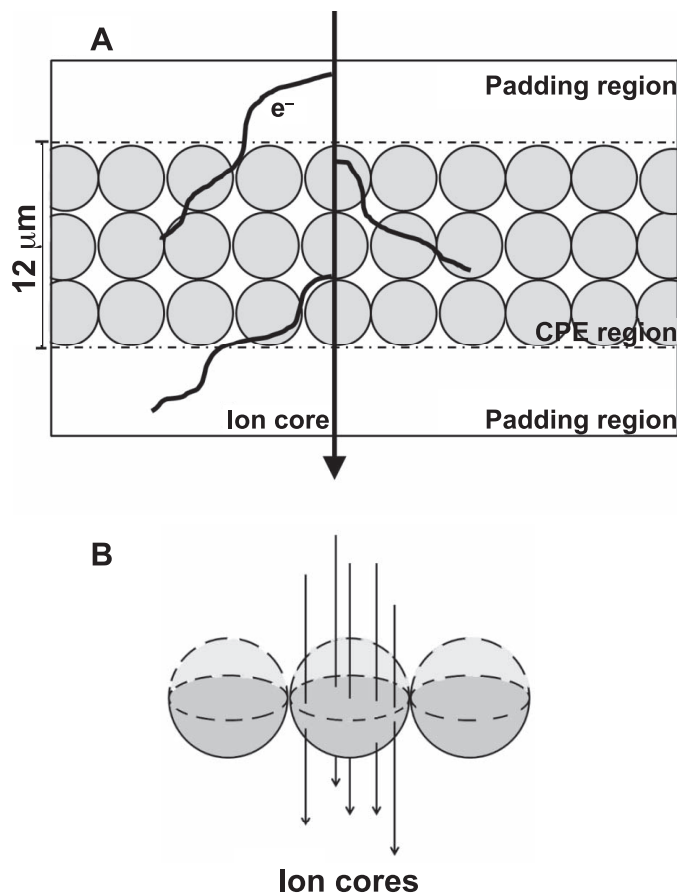


**FIG. 1.** Schematic representation of the scoring of  $f_i(z)$  for the proton and carbon-ion tracks. Each particle was transported event-by-event in a water phantom such that a 12- $\mu\text{m}$ -thick longitudinal charged particle equilibrium (CPE) region was achieved for the secondary electrons. At the center of this layer, the nominal energies of the tracks were the same as in Table 1. Panel A: The scoring of  $f_i(z)$  comprises both the track core and secondary electrons that traversed any of the spheres within the scoring layer. The spheres could have diameters up to 12  $\mu\text{m}$ . Panel B: The track positions were randomly distributed across the projected area of the “middle” spheres.

able with today’s biotechniques, and therefore an issue open for debate. For these types of models, knowledge of the size of such a target is crucial, since it represents a way towards characterizing radiation according to either the distribution of energy deposition, or the spatial distribution of the points of interaction (e.g., ionization clusters) within such targets.

In this work we explore the influence of target size variation on microdosimetric energy deposition distributions and the effect it may have on cell survival LQ parameterization. The dose-dependent frequency distribution of specific energy  $f(z,D)$  provides a full microscopic description of the distribution of energy deposition in a population of targets as a function of the average dose (10). This makes  $f(z,D)$  a candidate for use in the estimation of biological response at a subcellular level.

## MATERIALS AND METHODS

### Track Structure Simulations

A set of 500 proton and carbon-ion tracks (where a track consists of the primary particle together with its entire secondary particle cascade) was simulated in a water phantom with the updated version (11) of the Monte Carlo (MC) track structure code LIonTrack (12). To cover the thickness variation among healthy and cancerous mammalian cell nuclei, each particle track, starting from a unidirectional point source, was scored along a 12- $\mu\text{m}$ -long segment without lateral restriction. Longitudinal equilibrium of the released secondary electrons along this segment was provided by starting the particle at the top of a padding layer upstream and stopping the particle at the end of a second padding layer downstream of the 12- $\mu\text{m}$  scoring layer (see Fig. 1A). At the center of the scoring layer the nominal energies were 0.91, 1.40, 1.72, 3.18, 3.59 and 4.97  $\text{MeV}\text{u}^{-1}$  for the protons and 5.27, 10.95 and 76.9  $\text{MeV}\text{u}^{-1}$  for the carbon ions. Such energies correspond to those at which the referenced cell survival experiments (see Table 1) were performed. The transport cut-off energy of all secondary electrons was set at 50 eV, whereas the electron production cut-off was 1 eV, which is the lowest energy in the tabulated cross sections used by LIonTrack. Thus, any electron produced with or reaching a kinetic energy below the transport cut-off was not transported further and its energy was deposited on the spot. The energy deposition (ED) profile consisting of the coordinates where the EDs (ionizations and/or excitations) took place was tallied in separate files, one per simulated ion track. For the

**TABLE 1**  
Published LQ Alpha ( $\alpha$ ) and Beta ( $\beta$ ) Parameters from Experimentally Obtained Survival Curves for V79 Cell Line

Radiation quality	Mean energy/energy (MeV/MeV $\text{u}^{-1}$ )	$\alpha$ (Gy $^{-1}$ )	$\beta$ (Gy $^{-2}$ )	LET <sup>a</sup> (keV/ $\mu\text{m}$ )	Ref.
$^{60}\text{Co}$	1.25	$0.188 \pm 0.019$	$0.029 \pm 0.002$	0.2	(15)
H $^{+}$	0.91	$0.740 \pm 0.025$	$0.011 \pm 0.004$	27.6	(16)
H $^{+}$	1.4	$0.469 \pm 0.029$	$0.043 \pm 0.009$	20.0	(17)
H $^{+}$	1.72	$0.450 \pm 0.035$	$0.028 \pm 0.006$	17.8	(16)
H $^{+}$	3.18	$0.372 \pm 0.032$	$0.036 \pm 0.009$	11.0	(17)
H $^{+}$	3.59	$0.320 \pm 0.058$	$0.039 \pm 0.011$	10.1	(16)
H $^{+}$	4.97	$0.289 \pm 0.023$	$0.024 \pm 0.006$	7.70	(17)
C $^{6+}$	5.27	$0.99 \pm 0.081$	$-0.022 \pm 0.02^b$	275.1	(18)
C $^{6+}$	10.95	$0.91 \pm 0.096$	$0.044 \pm 0.033$	153.5	(18)
C $^{6+}$	76.9	$0.337 \pm 0.073$	$0.025 \pm 0.011$	32.40	(18)

*Note.* According to the references cited, LQ values are the result of averaging at least three independent experiments and thus, the associated uncertainty equals one standard deviation.

<sup>a</sup> LET values are as stated in the indicated references. For  $^{60}\text{Co}$  the value corresponds to LET<sub>d</sub>.

<sup>b</sup> In this work the  $\beta$  value is taken to equal to zero.

$^{60}\text{Co}$  source, a monoenergetic 1.25 MeV photon beam was used for the release of electron tracks in liquid water using an isotropic point source. No scattered photons were considered because in *in vitro* irradiation conditions their production is minimal, thus making their contribution to biological damage negligible.

#### Microdosimetric Background

The distribution of a sum of uncorrelated stochastic variables equals the convolution of their distributions. Therefore, the accumulation of dose in a microscopic subregion affected by a certain number of tracks can be derived by repeatedly convolving the frequency distribution of specific energy for one track  $f_1(z)$  with itself until the number of tracks  $v$  is reached. The mean  $\bar{z}_1$  of  $f_1(z)$  represents the mean specific energy that one track would deposit in the target volume and therefore the mean number of tracks  $n$  that would yield a dose is estimated by  $n = D/\bar{z}_1$ . Assuming that the number of tracks is Poisson distributed, the dose-dependent frequency distribution of specific energy is given by Kellerer and Chmelevsky (10) as:

$$f(z, D) = \sum_{v=0}^{\infty} e^{-n} \frac{n^v}{v!} f_v(z). \quad (2)$$

Equation (2) has two distinct components: 1. The first is a Poisson distribution  $e^{-n}n^v/v!$ , giving the probability that  $v$  tracks will contribute to the total dose  $D$  when the mean number of tracks is equal to  $n$ ; 2. The frequency distribution of specific energy for  $v$  tracks  $f_v(z) = \int_0^{\max} f_{v-1}(z-z')f_1(z')dz'$ , which gives the probability for a certain amount of energy to be imparted by exactly  $v$  tracks in a specified target. By definition, the mean of  $f(z, D)$  is equal to  $D$ .

Importantly,  $f_1(z)$  and all quantities derived from it are dependent on target size.

#### Calculation of $f_1(z)$ and $f(z, D)$

The  $f_1(z)$  distributions for protons and carbon ions were calculated by dividing the scoring layer described above, into layers of thickness equal to the diameter of the target volume. Each layer was filled with a grid of spheres with matching diameters while making sure that the track's core would traverse the center of the "middle" sphere at each layer, as shown in Fig. 1A. As a mean of variance reduction technique, the generated tracks were translated laterally to random positions across the projected area of the middle spheres (as shown in Fig. 1B) to reproduce the correct chord length distribution of tracks traversing a convex target at different positions. Each of the 500 simulated tracks was translated to 100 random positions, achieving a statistical uncertainty less than 1.5%. According to the reciprocity theorem [e.g., Attix (13)], this setup allows scoring of energy deposition not only by the track's core in the middle spheres but also from secondary electrons that traverse any of the surrounding spheres. Repeating the scoring procedure after each translation of the track yields a histogram which, after conversion of the deposited energy to specific energy, results in the  $f_1(z)$  distribution. This process was repeated for spheres with diameters ranging from 0.01 to 12  $\mu\text{m}$ .

A different approach was needed for the  $^{60}\text{Co}$  source because of the tortuous trajectories of the produced electrons. We applied the same procedure as used by Villegas *et al.* (14) for calculation of  $f_1(z)$  distributions where the volume of a bounding box enclosing each track (starting from a point source immersed in water) was divided into a grid of cubic sub-volumes of the desired size and for which the energy deposition was scored separately. However, two changes were applied. The first consisted of exchanging the scoring volumes from cubes to spheres. The second was to randomize the starting position of the first electron interaction within the spherical sub-volume in which it was found, thus avoiding bias in energy deposition within such sub-volume. Translation of the entire track was done accordingly. A total of 20,000 electron tracks were used to reach an acceptable statistical uncertainty.

For each of the spherical volumes,  $f(z, D)$  was determined according to Eq. (2) for doses between 1–6 Gy at 1 Gy intervals, thus covering the range of doses at which the published experimental survival assays were performed and whose LQ parameters will be used for later analysis (see Table 1). The convolutions of  $f_1(z)$  to yield  $f_v(z)$  were implemented using Mathematica™ version 11.1 (Wolfram Research Inc., Champaign, IL) cf. Villegas *et al.* (14). For some energies, the Poisson probability for  $v=0$  had the dominating weight factor, and to maintain normalization of  $f(z, D)$ , Eq. (2) was implemented with  $f_0(z)$  set to a Dirac delta distribution at  $z=0$ .

#### Cell Survival Fraction and Microdosimetry

The clonogenic cell survival assay provides a simple method for quantifying survival fractions,  $\text{SF}(D)$ . Essentially, the fraction of cells that manages to proliferate from independently exposed populations to various dose levels is quantified. Recalling from the microdosimetry theory that the energy deposited in each individual cell is governed by  $f(z, D)$ , where  $D$  is the dose given to the cell population, and assuming the existence of a survival fraction  $\text{SF}(z)$ , where cells receiving equal  $z$  have equal probability of mortality, we can hypothesize that the  $\text{SF}(D)$  can be described by:

$$\text{SF}(D) = \int_0^{\infty} f(z, D) \text{SF}(z) dz. \quad (3)$$

In other words,  $\text{SF}(D)$  for any cell population can be interpreted as the average of the individual  $\text{SF}(z)$  weighted by the physical properties of the radiation expressed as  $f(z, D)$ . The assumption behind Eq. (3) is indeed the most basic in terms of modeling, namely that biological response is governed by the specific energy received and that the biological effect exhibited by the irradiated cells is independent of the effect on the others (i.e., no bystander effect). Yet, for the purpose of this work, it is ideal to express the survival fraction as in Eq. (3) because it opens the possibility to directly study the influence of target size on biological response, as  $f(z, D)$  hinges on target size. Following Poisson statistics,  $\text{SF}(z)$  can be described by  $e^{-az}$ , where parameter  $a$  represents the mean number of lethal events per specific energy, yielding:

$$\text{SF}(D) = \int_0^{\infty} f(z, D) e^{-az} dz. \quad (4)$$

To study the behavior of the parameter  $a$  as a function of target size, we make use of experimentally derived  $\text{SF}(D)$  approximated by LQ parameterization. For the following analysis we use only the linear term, as it describes  $\text{SF}(D)$  at fraction doses that are clinically relevant in ion therapy. Values for the parameter  $a$  can thus be fitted by minimizing the following objective function:

$$\{a_{\text{fit}}\} = \text{ArgMin} \int \left( e^{-aD} - \int_0^{\infty} f(z, D) e^{-az} dz \right)^2 dD. \quad (5)$$

In practice, the  $f(z, D)$  frequencies present intrinsic noise, which makes brute-force integration challenging. To facilitate computations, we instead make use of the cumulative dose-dependent specific energy function  $F(z, D) = \int_0^z f(z', D) dz'$ , which enables application of the integration by parts yielding:

$$\int_0^{\infty} f(z', D) e^{-az'} dz' = a \int_0^{\infty} F(z', D) e^{-az'} dz'. \quad (6)$$

Note that the lower limit of the integrals in Eq. (6) includes full integration the Dirac pulse at  $z=0$  in  $f(z, D)$ . Mathematically, the lower limit should be marked as  $0^-$ , however, since negative values of  $z$  have



no physical significance, we kept the notation with 0 as the limit. The right-hand side integral of Eq. (6) can be further divided into two separate ranges; the first is  $[0, z_{\max}]$ , where  $z_{\max}$  is the maximum tabulated value of  $F(z, D)$  and the second being  $[z_{\max}, \infty]$  for which the evaluation of  $F(z, D)$  is by definition equal to unity. Therefore, Eq. (6) becomes:

$$\int_0^\infty f(z', D)e^{-az'} dz' = a \left( \int_0^{z_{\max}} F(z', D)e^{-az'} dz' + \int_{z_{\max}}^\infty e^{-az'} dz' \right). \quad (7)$$

Substitution of Eq. (7) into Eq. (5) yields the final objective function

$$\begin{aligned} & \{a_{\text{fit}}\} \\ & = \text{ArgMin} \\ & \int \left( e^{-zD} - a \left( \int_0^{z_{\max}} F(z', D)e^{-az'} dz' + \int_{z_{\max}}^\infty e^{-az'} dz' \right) \right)^2 dD, \quad (8) \end{aligned}$$

which was evaluated by an in-house code developed in Mathematica™ using its FindMinimum algorithm.

A data set of 10 *in vitro* experimental survival curves for the Chinese hamster lung cell line V79 was selected from the literature. Each survival curve corresponds to exposure to different radiation types varying in energy: 6 protons, 3 carbon ions and <sup>60</sup>Co photons. Both of the LQ parameters are shown in Table 1.

## RESULTS

### The Distributions $f_1(z)$ and $f(z, D)$

Examples of the calculated  $f_1(z)$  distributions are shown in Fig. 2. At a diameter of 0.01 μm the  $f_1(z)$  rapidly decreases with  $z$  in more or less the same pace for all radiation species and energies; however, for the lowest carbon ion (5.27 MeVu<sup>-1</sup>) a distinct peak is observed at approximately  $3 \times 10^5$  Gy. This peak becomes distinctively triangular as the target volume increases. Likewise,  $f_1(z)$  for all ions (protons and carbons) presents such a characteristic triangular shape at some given target size. This behavior is a hallmark of the chord length distributions resulting from straight track segments traversing a sphere. Thus, the triangular part of  $f_1(z)$  is due to the track cores, whereas the structures at low specific energies are due to the delta electron tracks. On the other hand, the absence of the triangular pattern at any target size in the  $f_1(z)$  of the <sup>60</sup>Co comes as a result of the tortuous path of the electron tracks. The triangular part of  $f_1(z)$  shifts to lower  $z$  values with increasing particle energy.

The resulting  $f(z, D)$  for  $D$  equal to 1 and 5 Gy are shown in Fig. 3 for spheres with diameters of 0.01, 0.5 and 10 μm. The distinctive triangular shape seen in some  $f(z, D)$  curves are reminiscent of the triangle observed in  $f_1(z)$  for protons and carbon ions. For these cases, the mean number of tracks  $n$  is approximately one, causing  $f(z, D)$  to be essentially equal to  $f_1(z)$  renormalized by the Poisson factor of Eq. (2). It is important to point out that when  $n \ll 1$ , the dominant term of the  $f(z, D)$  distribution is the no-hit term i.e.,  $f(z = 0, D)$ . At this point it is much more likely that the particle track will miss the target entirely than to hit it. But if a hit occurs, the deposited specific energy can exceed up to 5

orders of magnitude of the mean dose (see the cases of the 0.01- and 0.5-μm diameter spheres shown in Fig. 3).

If either the target size or the mean dose is increased, the number of convolutions in Eq. (2) also increases, eventually causing  $f(z, D)$  to become normally distributed around the mean  $\bar{z} = D$  regardless of radiation quality. The actual target size or mean dose at which such transition occurs can vary from one quality to another. In Fig. 3 it can be observed that 1 Gy given to a 10-μm diameter sphere, the  $f(z, D)$  is normally distributed (note that the log-log plot causes a visual skewness of symmetric distributions) when irradiated by <sup>60</sup>Co or 0.91 MeVu<sup>-1</sup> protons but not when irradiated by 5.27 MeVu<sup>-1</sup> carbon ions. If the dose increases above 5 Gy then  $f(z, D)$  becomes normally distributed for these carbon ions.

### Fitting of the LQ Parameter

The behavior of the parameter  $a_{\text{fit}}$  in Eq. (4) as a function of target diameter for different radiation species was explored by fitting to available experimental values of  $\alpha$ . The results expressed as the ratio  $a_{\text{fit}}/\alpha_{\text{exp}}$  for <sup>60</sup>Co, 0.91 MeVu<sup>-1</sup> protons, and 76.90 and 5.27 MeVu<sup>-1</sup> carbon ions are shown in Fig. 4. As expected, this ratio tends towards unity with increasing diameter regardless of radiation species, but the target size at which the ratio reaches unity varies with radiation quality. For <sup>60</sup>Co, a 2-μm diameter sphere is sufficient to provide equality (less than 1% difference) between parameter  $a_{\text{fit}}$  and  $\alpha$ , whereas for the lowest carbon energy the ratio is approximately 1.3 for a 12-μm diameter sphere.

More interestingly, our results demonstrate the existence of a threshold in target size below which there is no satisfactory fit of Eq. (5) as the residuals become too large ( $\gg 10$ -fold). This is indicated in Fig. 4 by the dashed lines. It can also be observed that such threshold size varies among radiation qualities. Our results show that the threshold size for <sup>60</sup>Co [lowest linear energy transfer (LET) radiation in this work] is between 0.1 and 0.5 μm. As LET increases, so does the threshold size, reaching between 6 and 7 μm for 5.27 MeVu<sup>-1</sup> carbon ions (highest LET radiation in this work).

### Microdosimetric Restriction on the Sensitive Volume

The existence of a threshold size discussed in the previous section is closely related to an intrinsic geometrical limit imposed by the microdosimetric formalism [e.g. (19)]. Under the assumption that cells are autonomous, the survival fraction is the conditional probability of survival  $P(S)$  given the probability of no-hit  $P(\text{NH})$  (the probability that a cell is missed by a particle and/or its secondaries) and the probability of hit and repair  $P(\text{HR})$  (the probability that a cell hit by the particle and/or its secondaries survives as a result of a successful damage repair), i.e.,

$$\text{SF} = P(S|\text{NH} \vee \text{HR}). \quad (9)$$

Recalling that  $n$  is the mean number of tracks passing through a target exposed to a mean dose  $D$ , then  $P(\text{NH})$  is

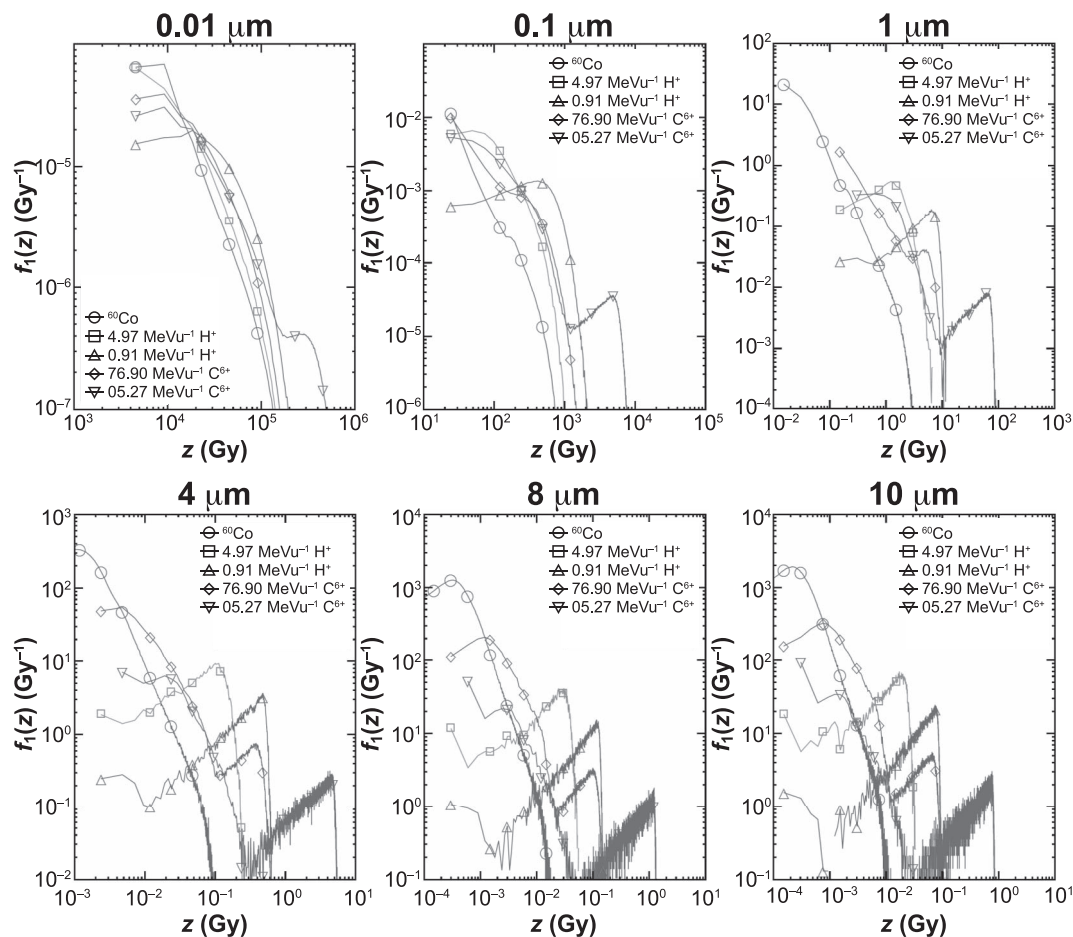


**FIG. 2.** Frequency distribution of specific energy for one track  $f_1(z)$  calculated for spheres with indicated diameters, from 0.01–10.0  $\mu\text{m}$ , for  $^{60}\text{Co}$ , 4.97  $\text{MeVur}^{-1}$  protons, 0.91  $\text{MeVur}^{-1}$  protons, 76.9  $\text{MeVur}^{-1}$  carbon ions and 5.27  $\text{MeVur}^{-1}$  carbon ions.

numerically equal to the Poisson probability with  $\nu = 0$  (no tracks), i.e.,  $P(\text{NH}) = e^{-n}$ . It is worth noting that  $P(\text{NH})$  can also be extracted by integrating the surviving term of  $f(z, D)$  when setting  $\nu = 0$ , i.e.,  $P(\text{NH}) = \int_0^{\infty} e^{-n} f_0(z) dz$ . Since  $f_0(z)$  is a Dirac delta distribution at  $z = 0$ , the integral will yield the same result.

Comparison between the no-hit probability as a function of dose for different target sizes with the  $\text{SF}(D)$  clearly illustrates the existence of a lower limit in size of the sensitive volume within a cell. Namely, target sizes whose  $P(\text{NH})$  curves are greater than the experimentally measured  $\text{SF}(D)$  violate Eq. (9) and cannot be used to describe the linear term of  $\text{SF}(D)$ . Figure 5 shows such comparison for V79 cells. As expected, the slope of the  $P(\text{NH})$  curves increases with decreasing volume indicating that smaller targets are easier to miss, regardless of radiation quality. Yet, the limit in sensitive size varies with the microdosimetric characteristics of the ionizing radiation tracks, e.g., increasing limit size with decreasing initial kinetic energy of the particle.

The range of limits described in this section is equivalent to the range of threshold sizes found by the fitting process in the previous section. This similarity is clear evidence that the single track microdosimetric distribution of energy deposition in relationship to the size of the available sensitive size within a cell affects, to some extent, the probability of survival of the cell.

#### Mean Inactivation Dose

The mean inactivation dose (MID), defined as the area under the survival curve,

$$\text{MID} = \int_0^{\infty} \text{SF}(D) dD, \quad (10)$$

can be interpreted as the dose needed to cause on average one lethal event (19). Dividing MID by  $z_1$  (mean specific energy deposited by the passage of one track) will yield the mean number of inactivation tracks,  $m$ . In other words,  $m$  is the fraction of  $n$  (defined in the microdosimetric background section), that will cause (on average) a lethal event. It

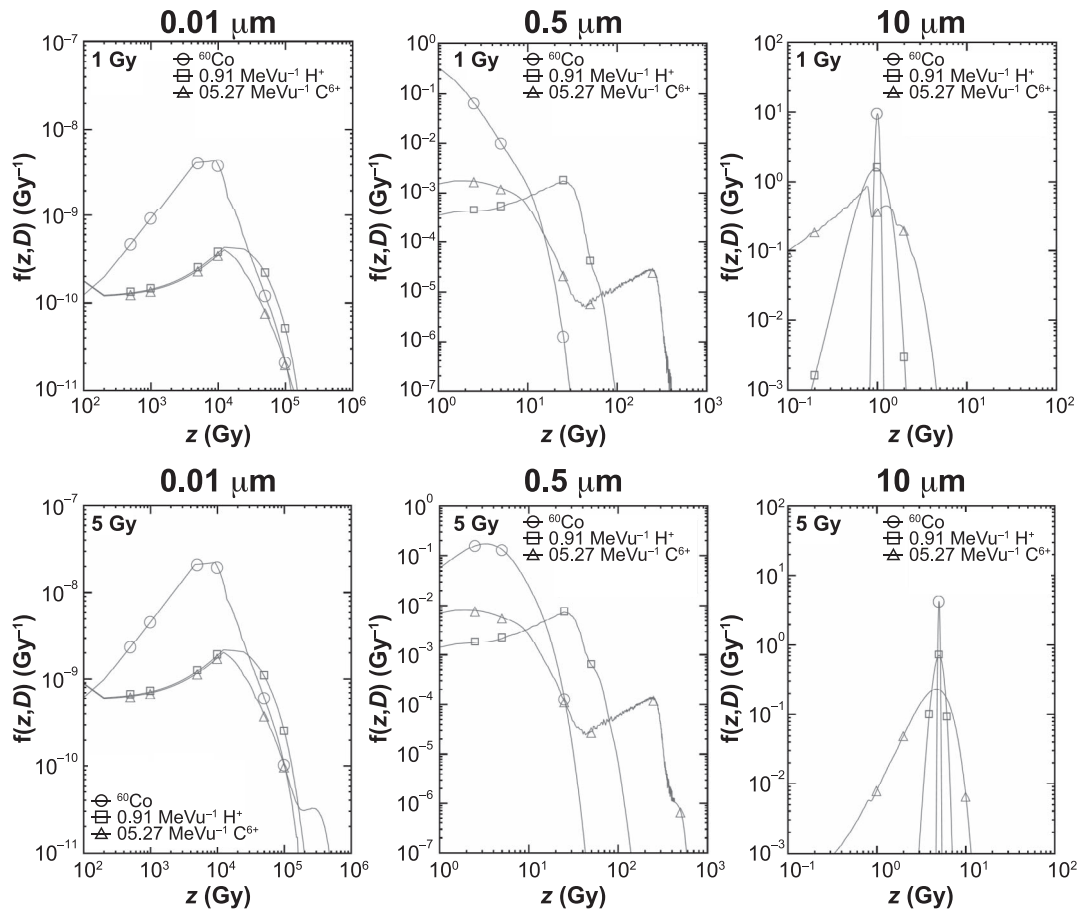


**FIG. 3.** Dose-dependent frequency distribution of specific energy  $f(z,D)$  for spheres with diameters of 0.01, 0.5, and 10  $\mu\text{m}$  for doses of 1 and 5 Gy for  $^{60}\text{Co}$ , 0.91  $\text{MeVu}^{-1}$  protons and 5.27  $\text{MeVu}^{-1}$  carbon ions. The distributions were calculated according to Eq. (2). Note that the no-hit peak is not shown in all log-log scale plots.

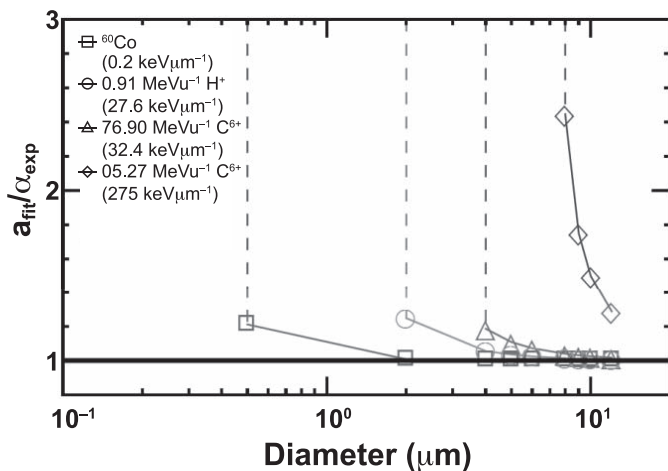


**FIG. 4.** The ratio of  $a_{\text{fit}}/a_{\text{exp}}$  as a function of diameter size is shown for  $^{60}\text{Co}$ , 0.91  $\text{MeVu}^{-1}$  protons and 76.90 and 5.27  $\text{MeVu}^{-1}$  carbon ions. The threshold size below which Eq. (5) fails to fit is given by the marker at the joints of the dashed and continuous lines. All lines in the plot serve only as a guide for the eye.

follows that the volume at which one track is expected to become lethal can be estimated by looking for the target size at which  $\bar{z}_1$  equals the MID (i.e.,  $m = 1$ ). Following the results of the previous sections, it is anticipated that this “single-track lethal-volume” also varies with radiation quality. Knowledge of this volume enables the calculation of a special frequency-mean lineal energy  $\bar{y}_{f,\text{MID}}$  for which the sizes are tuned to yield  $m = 1$  and can thus be seen as a radiobiological property of the radiation quality. From here on, we will use the sub-index MID to emphasize that those values of  $\bar{y}_f$  have been calculated with such target sizes.

In this work, calculation of  $\bar{y}_{f,\text{MID}}$  values started by extracting the functions  $\bar{z}_1(d)$  and  $\bar{y}_{f,(d)}$  ( $d$  being the diameter of spherical targets) from the set of  $f_i(z)$  frequencies calculated via MC simulations (see Materials and Methods) for the various radiation qualities. The MID values were calculated with Eq. (10) employing the experimental LQ parameters given in Table 1. Then, the  $\bar{z}_1(d)$  function was searched for the condition  $m = 1$  to obtain the diameter of the “single-track lethal-volume” per radiation quality. Finally, the corresponding  $\bar{y}_{f,(d)}$  functions were evaluated at such diameters to acquire the desired  $\bar{y}_{f,\text{MID}}$  values.

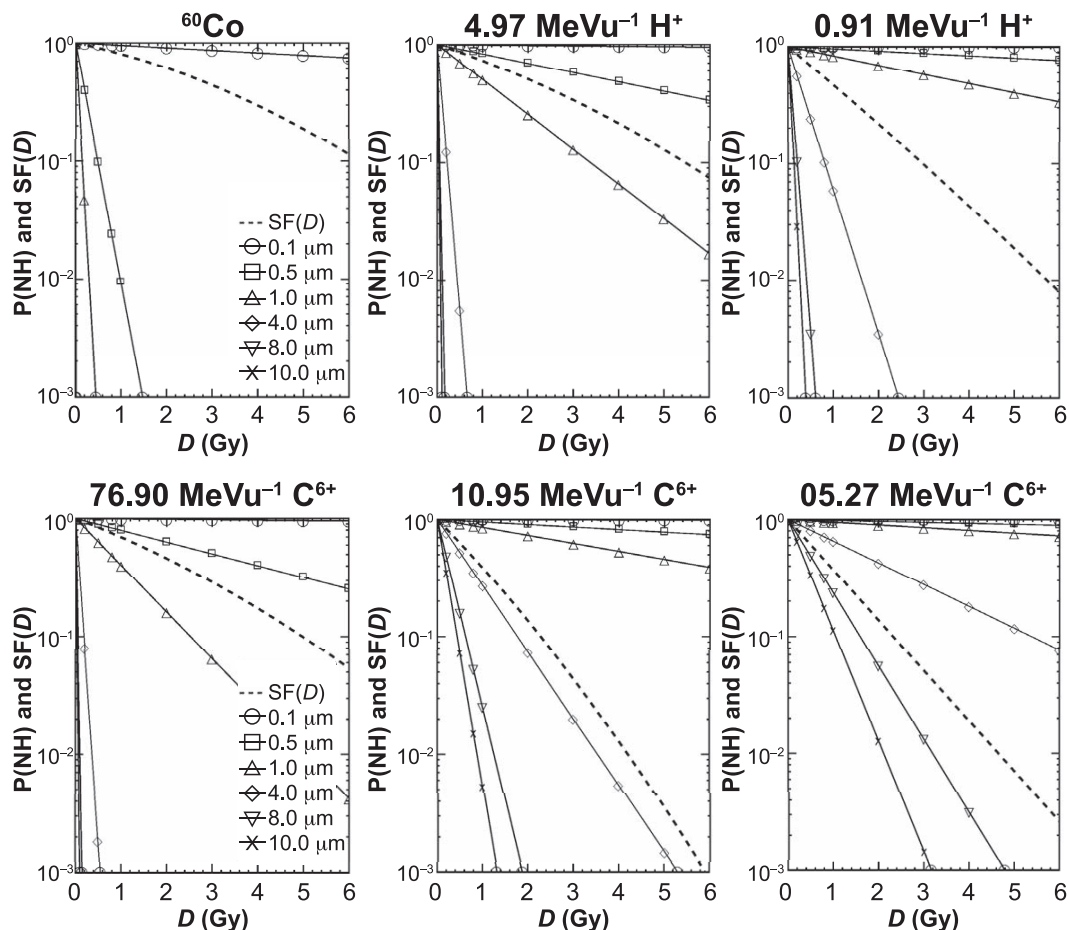


**FIG. 5.** Comparison of survival fraction  $SF(D)$  (dashed line) with the no-hit probabilities  $P(NH)$  (various symbols) as a function of dose for target sizes varying in diameter from  $0.1 \mu\text{m}$  to  $10 \mu\text{m}$  for  $^{60}\text{Co}$ , the lowest and highest proton energies and all carbon-ion energies from Table 1.

Figure 6 shows the diameter and the deposited energy of the “single-track lethal-volume” as a function of  $\bar{y}_{f,\text{MID}}$ . The smooth increase of both curves observed across radiation species is noteworthy. Both curves can be easily parameterized by a relationship of the type  $k \cdot (\bar{y}_{f,\text{MID}})^p$ , which suggests that  $\bar{y}_{f,\text{MID}}$  could be a potential candidate for radiation quality characterization for modeling. It is worth pointing out that such characterization is limited to the biological conditions under which the clonogenic assay has been performed, thus, the results in Fig. 6 apply only for V79 cells.

## DISCUSSION

All microdosimetric quantities are target size dependent. This represents a hindrance for radiobiological models based on micro- and nanodosimetry as the actual sensitive volume sizes within a cell cannot be experimentally determined. However, radiobiological models like the fourth version of the local effect model (LEM IV) (20), Katz’s track structure model (21) and the modified microdosimetric kinetic model (mMKM) (22) assume that the

critical target is found within the cell nucleus (micrometer size) and that this target can be further divided into small independent nanometer-sized sub-volumes. In these models, cell survival depends on the accumulated severity of the lesions within the sub-volumes, often referred to as domains. Accordingly, the key to modeling survival curves is to find a relationship between the lesions and distribution of energy deposition within the domain. Therefore, most modeling work would benefit from correct estimates of the domain’s volume. Meanwhile, the parameter for “cell nucleus target” volume plays a minor role, appearing as a fixed value in the above mentioned, as well as other more recent, modeling approaches (23–25). The results of this work suggest that a more accurate estimation of the size of this target can be calculated and that perhaps such volume plays role that is equally as important as that of the domain because of its relationship with the ionizing radiation’s probability of interaction. Indeed, the relevance of such probability (in the form of the action cross section) is hinted at in Katz’s track structure model (21), as it directly determines the “ion-kill” component of the cell survival fraction. The “gamma-kill” component is, however,



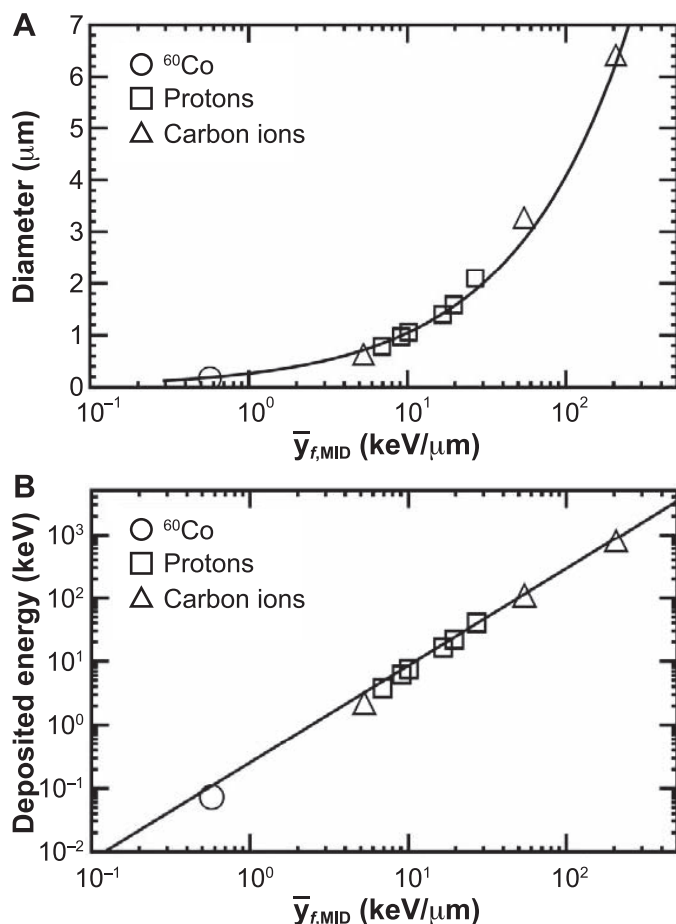


**FIG. 6.** The diameters (panel A) and the energy deposited (panel B) in the “single-track lethal-volume” as a function of  $y_{f,MID}$  for the radiation qualities shown in Table 1. The results shown here were parameterized with the expression of the form  $k \cdot (y_{f,MID})^p$ . If  $y_{f,MID}$  is given in  $\text{keV}\mu\text{m}^{-1}$ , diameter in  $\mu\text{m}$  and deposited energy in keV, then values found for the parameters  $k$  and  $p$  were 0.27 and 0.6 in panel A, whereas in panel B the values were 0.25 and 1.5, respectively.

dependent on a fitted value of the geometrical cross section of the cell nucleus target.

The hypothesis behind this study is that the expected biological effect (e.g., measured by  $SF(D)$ ) is a result of the averaging of the individual effects caused by the radiation’s intrinsic variation of energy deposition (e.g., specific energy) at the level of subcellular volumes. Thus, the natural candidate for expressing the  $SF(D)$  under these terms is the  $f(z,D)$  distribution because it explicitly describes the probability of energy deposition for a given target size and given mean dose [see Eq. (4)]. The biological effect in Eq. (4) is carried by the parameter  $a$  and it is expected to exert its effect solely on the sensitive volume of the cell. To find the parameter value of  $a$ , a fitting process to published experimental survival curves was performed. For each radiation quality tested here, a range of target sizes yielded suitable  $a_{fit}$  values through the application of Eq. (8). Figure 4 shows that as target size increases, the value of  $a_{fit}$  approximates the experimental LQ value of  $\alpha$  for all radiation qualities, albeit at different rates. Indeed, at larger

volumes,  $f(z,D)$  becomes normally distributed around the mean dose  $D$  with a small enough spread that translates, within our hypothesis frame, into an almost negligible difference between the cell’s individual biological effect and the mean overall effect.

Although no further mechanistic conclusions can be drawn from this behavior, our study revealed the existence of a threshold in target size below which the fit fails. More interestingly is that these threshold sizes may significantly vary between radiation species (spheres with diameters between 0.1 and 0.5  $\mu\text{m}$  for <sup>60</sup>Co to diameters between 6 to 7  $\mu\text{m}$  for carbon ions). The mathematical reason for the lack in the goodness-of-fit is that at the threshold size the first term of the  $f(z,D)$  summation [i.e.,  $f_0(z)e^{-z}$ ] becomes the dominating factor, especially at low doses (generally below 3 Gy for the ion energies tested here). Consequently, there is no valid  $a_{fit}$  value that can satisfy Eq. (8) across the dose levels commonly used in cell survival experiments.

At first, this finding seems to challenge the assumption that cells have a unique sensitive volume. However, the notion of a limit in sensitive volume that varies with radiation quality comes out naturally from the mathematical constraint that the probability of no-hit at each dose has to be less than or equal to the probability of cell survival (see Results). Essentially, the relationship between the microdosimetric distribution of energy deposition (which is a property of radiation quality that changes with target size) and the measured cell survival sets a minimum (threshold) volume within a cell that the ionizing track should affect, to cause a lethal effect. This concept directly influences the modeling of the initial slope of the survival curve (e.g.,  $\alpha$  parameter) because it is closely related to the lethal potential of the single-track hit. Published models for heavy ions such as LEM IV [e.g., (26)], the mMKM model [e.g., (27)] and multi-hit single-target model (28) agree well with experimental survival data when using cell nucleus target volumes corresponding to spheres with diameters between 6 and 8  $\mu\text{m}$ . These volumes are in agreement with our estimated threshold volume for the lowest-energy carbon ion. This suggests that regardless of the model’s theoretical framework, to model data for lower-energy particles, it is necessary to introduce a target that is at least the size of its threshold volume. Data for particles of higher energy will be naturally covered as the threshold volume decreases with increasing particle energy. It is also important to clarify that the cell nucleus target does not necessarily equal the visible size of the cell’s nucleus, as shown by Hawkins (29) for V79 cells in different stages of the cell cycle.

Additionally, we calculated the magnitude of such threshold volume by finding the target size at which the mean specific energy for one track  $\bar{z}_1$  equals the MID. Thus, the threshold volume can be interpreted as the volume that, if hit by one track, will provoke a lethal event in the cell. The diameters of these spherical volumes were then used to calculate a special kind of mean lineal energy  $\bar{y}_{f,MID}$ , which can be regarded as a radiobiological property characteristic of

radiation quality. The surprisingly smooth curves that result from characterizing radiation quality by its  $\bar{y}_{f,MID}$  values (see Fig. 6) hints at the property's potential in modeling. Microdosimetric measurements of mean specific energy as a function of target size can be readily obtained for hadron-therapy beams by using state-of-the-art detectors. These measurements, coupled to a consistent cell survival database, would yield  $y_{f,MID}$  values that can characterize mixed field beams at various depths. Moreover, such experimental output can provide a reliable benchmarking of Monte Carlo codes.

## CONCLUSION

The spatial distribution of energy deposition as described by  $f(z,D)$  is notably influenced by changes in target size. The no-hit peak becomes the dominant factor as volume decreases for any radiation quality. This behavior imposes a natural limit on the possible sensitive size (at the cell nucleus level) of the cell when its relationship with cell survival data is studied. Moreover, such a threshold volume is radiation quality-dependent, increasing with decreasing particle energy. This finding led to the derivation of a potentially useful microdosimetric property  $\bar{y}_{f,MID}$ , which characterizes ionizing radiation across radiation modalities in relationship to their cell inactivation capacities.

## ACKNOWLEDGMENTS

We gratefully acknowledge the Swedish Radiation Safety Authority (SSM) for their financial support. The computations were performed on resources provided by SNIC through the Uppsala Multidisciplinary Centre for Advanced Computational Science (UPPMAX) under project nos. p2011144 and snic2016-7-92.

Received: March 16, 2018; accepted: July 10, 2018; published online: August 14, 2018

## REFERENCES

- Chadwick KH, Leenhouts HP. A molecular theory of cell survival. *Phys Med Biol* 1973; 18:78–87.
- Schardt D, Elsasser T, Schulz-Ertner D. Heavy-ion tumor therapy: Physical and radiobiological benefits. *Rev Mod Phys* 2010; 82:383–425.
- Amaldi U, Kraft G. Radiotherapy with beams of carbon ions. *Rep Prog Phys* 2005; 68:1861–82.
- Prescribing, recording, and reporting proton-beam therapy. ICRU Report No. 78. Bethesda, MD: International Commission on Radiation Units and Measurements; 2007.
- Tilly N, Johansson J, Isacson U, Medin J, Blomquist E, Grusell E, et al. The influence of RBE variations in a clinical proton treatment plan for a hypopharynx cancer. *Phys Med Biol* 2005; 50:2765–77.
- Frese MC, Wilkens JJ, Huber PE, Jensen AD, Oelfke U, Taheri-Kadkhoda Z. Application of constant vs. variable relative biological effectiveness in treatment planning of intensity-modulated proton therapy. *Int J Radiat Oncol Biol Phys* 2011; 79:80–8.
- Dasu A, Toma-Dasu I. Impact of variable RBE on proton fractionation. *Med Phys* 2013; 40:011705.
- Kellerer AM, Rossi HH. A generalized formulation of dual radiation action. *Radiat Res* 1978; 75:471–88.
- Szumiel I. Ionizing radiation-induced oxidative stress, epigenetic changes and genomic instability: The pivotal role of mitochondria. *Int J Radiat Biol* 2015; 91:1–12.
- Kellerer AM, Chmelevsky D. Concepts of microdosimetry. II. Probability distributions of the microdosimetric variables. *Radiat Environ Biophys* 1975; 12:205–16.
- Villegas F, Ahnesjo A. Reply to the comment on 'Monte Carlo calculated microdosimetric spread for cell nucleus-sized targets exposed to brachytherapy  $^{125}\text{I}$  and  $^{192}\text{Ir}$  sources and  $^{60}\text{Co}$  cell irradiation'. *Phys Med Biol* 2016; 61:5103.
- Backstrom G, Galassi ME, Tilly N, Ahnesjo A, Fernandez-Varea JM. Track structure of protons and other light ions in liquid water: Applications of the LlonTrack code at the nanometer scale. *Med Phys* 2013; 40:064101.
- Attix FH. Introduction to radiological physics and radiation dosimetry. New York: John Wiley and Sons; 1986.
- Villegas F, Tilly N, Ahnesjo A. Monte Carlo calculated microdosimetric spread for cell nucleus-sized targets exposed to brachytherapy  $^{125}\text{I}$  and  $^{192}\text{Ir}$  sources and  $^{60}\text{Co}$  cell irradiation. *Phys Med Biol* 2013; 58:6149–62.
- Stenerlow B, Pettersson OA, Essand M, Blomquist E, Carlsson J. Irregular variations in radiation sensitivity when the linear energy transfer is increased. *Radiother Oncol* 1995; 36:133–42.
- Folkard M, Prise KM, Vojnovic B, Newman HC, Roper MJ, Michael BD. Inactivation of V79 cells by low-energy protons, deuterons and helium-3 ions. *Int J Radiat Biol* 1996; 69:729–38.
- Belli M, Cera F, Cherubini R, Dalla Vecchia M, Haqjue AMI, Ianzini F, et al. RBE-LET relationships for cell inactivation and mutation induced by low energy protons in V79 cells: Further results at the LNL facility. *Int J Radiat Biol* 1998; 74:501–9.
- Weyrather WK, Ritter S, Scholz M, Kraft G. RBE for carbon track-segment irradiation in cell lines of differing repair capacity. *Int J Radiat Biol* 1999; 75:1357–64.
- Rossi HH, Zaider M. Radiobiology. In: Rossi HH, Zaider M, editors. *Microdosimetry and its applications*. Berlin: Springer; 1996. p. 212–4.
- Elsasser T, Weyrather WK, Friedrich T, Durante M, Iancu G, Kramer M, et al. Quantification of the relative biological effectiveness for ion beam radiotherapy: Direct experimental comparison of proton and carbon ion beams and a novel approach for treatment planning. *Int J Radiat Oncol* 2010; 78:1177–83.
- Katz R. Biological effects of heavy ions from the standpoint of target theory. *Adv Space Res* 1986; 6:191–8.
- Kase Y, Kanai T, Matsumoto Y, Furusawa Y, Okamoto H, Asaba T, et al. Microdosimetric measurements and estimation of human cell survival for heavy-ion beams. *Radiat Res* 2006; 166:629–38.
- Ballarini F, Altieri S, Bortolussi S, Giroletti E, Protti N. A model of radiation-induced cell killing: Insights into mechanisms and applications for hadron therapy. *Radiat Res* 2013; 180:307–15.
- Cunha M, Monini C, Testa E, Beuve M. NanOx, a new model to predict cell survival in the context of particle therapy. *Phys Med Biol* 2017; 62:1248–68.
- McMahon SJ, McNamara AL, Schuemann J, Paganetti H, Prise KM. A general mechanistic model enables predictions of the biological effectiveness of different qualities of radiation. *Sci Rep* 2017; 7:10790.
- Friedrich T, Scholz U, Elsasser T, Durante M, Scholz M. Calculation of the biological effects of ion beams based on the microscopic spatial damage distribution pattern. *Int J Radiat Biol* 2012; 88:103–7.
- Kase Y, Kanai T, Matsufuji N, Furusawa Y, Elsasser T, Scholz M. Biophysical calculation of cell survival probabilities using amorphous track structure models for heavy-ion irradiation. *Phys Med Biol* 2008; 53:37–59.
- Vassiliev ON. Formulation of the multi-hit model with a non-Poisson distribution of hits. *Int J Radiat Oncol Biol Phys* 2012; 83:1311–6.
- Hawkins RB. A microdosimetric-kinetic model for the effect of non-Poisson distribution of lethal lesions on the variation of RBE with LET. *Radiat Res* 2003; 160:61–9.